

A Flux Model of Glycolysis and the Oxidative Pentosephosphate Pathway in Developing *Brassica napus* Embryos*

Received for publication, April 2, 2003
Published, JBC Papers in Press, May 20, 2003, DOI 10.1074/jbc.M303432200

Jörg Schwender[‡], John B. Ohlrogge, and Yair Shachar-Hill

From the Department of Plant Biology, Michigan State University, East Lansing, Michigan 48824

Developing oilseeds synthesize large quantities of triacylglycerol from sucrose and hexose. To understand the fluxes involved in this conversion, a quantitative metabolic flux model was developed and tested for the reaction network of glycolysis and the oxidative pentose phosphate pathway (OPPP). Developing *Brassica napus* embryos were cultured with [U - $^{13}C_6$]glucose, [1 - ^{13}C]glucose, [6 - ^{13}C]glucose, [U - $^{13}C_{12}$]sucrose, and/or [$1,2$ - $^{13}C_2$]glucose and the labeling patterns in amino acids, lipids, sucrose, and starch were measured by gas chromatography/mass spectrometry and NMR. Data were used to verify a reaction network of central carbon metabolism distributed between the cytosol and plastid. Computer simulation of the steady state distribution of isotopomers in intermediates of the glycolysis/OPPP network was used to fit metabolic flux parameters to the experimental data. The observed distribution of label in cytosolic and plastidic metabolites indicated that key intermediates of glycolysis and OPPP have similar labeling in these two compartments, suggesting rapid exchange of metabolites between these compartments compared with net fluxes into end products. Cycling between hexose phosphate and triose phosphate and reversible transketolase velocity were similar to net glycolytic flux, whereas reversible transaldolase velocity was minimal. Flux parameters were overdetermined by analyzing labeling in different metabolites and by using data from different labeling experiments, which increased the reliability of the findings. Net flux of glucose through the OPPP accounts for close to 10% of the total hexose influx into the embryo. Therefore, the reductant produced by the OPPP accounts for at most 44% of the NADPH and 22% of total reductant needed for fatty acid synthesis.

Brassica napus (rapeseed, canola) is one of the world's major oilseed crops and is also a well studied model for oilseed metabolism (1–21). The main storage compounds in seeds of *B. napus* are oil (triacylglycerols) and storage proteins, which are derived from sugars and amino acids taken up from the surrounding endosperm liquid (11, 12, 22, 23). Because of its high oil content and ease of genetic transformation, *B. napus*

has also been a target for metabolic engineering of oil metabolism. However, some attempts to engineer plant oils have had limited success (for a review, see Ref. 24). In order to make advances in improving oil yield and quality, a more detailed understanding of metabolism during seed development is needed. In particular, a number of fundamental metabolic issues remain unresolved. These include the source(s) of reductant and ATP for fatty acid synthesis; the degree to which cytosolic, plastidial, and mitochondrial metabolic fluxes are integrated; and the chief metabolic and transport route(s) by which carbon flows from maternal sources to seed storage products.

Fatty acid synthesis has a high demand for reductant, and in other systems there is evidence that the supply of reductant can limit lipid accumulation (25, 26). Thus, determining the source of reductant for fatty acid synthesis in developing oil seeds is important, and in particular the contribution of NADPH made by the oxidative pentose phosphate pathway (OPPP)¹ to fatty acid synthesis is not known. Of the two reducing steps of fatty acid synthesis, *in vitro* data indicate that the first (3-ketoacyl-ACP reductase; EC 1.1.1.100) requires NADPH (27), whereas the second (enoyl-ACP reductase, EC 1.3.1.9) requires NADH (28). NADH can be provided by the pyruvate dehydrogenase reaction in plastids, whereas it has long been thought that NADPH for reductive syntheses in nonphotosynthetic plastids is produced by the OPPP (29). However, reductant could also be provided by steps in glycolysis (*e.g.* GAP-dehydrogenase; EC 1.2.1.13), by photosystems of green seeds, or by the import into the plastid of reducing equivalents generated in the mitochondria or cytosol. Thus, the OPPP represents one of several possible sources of reductant for oil synthesis in seeds, and the *in vivo* contribution of these alternatives has not been established.

In recent years, it has become clear that measuring fluxes through the OPPP presents technical challenges and requires careful experimental design and interpretation. The effects of cycling among hexose, triose, and pentose pools via reversible reactions leads to label redistributions that must be quantitatively considered if one is to understand the sources of carbon and reductant (30). Understanding flux through metabolic networks that involve reversible, branching, and parallel pathways has been greatly aided by the development of steady state labeling methods using stable isotopes and isotopomer analysis (31–34). Analysis of isotopomer distributions in intermediates

* This work was supported by Department of Energy Grant DE-FG02-87ER13729, National Science Foundation Grant MCB 0224655, and United States Department of Agriculture Grant 83786. This work was also supported by the Michigan Agricultural Experiment Station. The costs of publication of this article were defrayed in part by the payment of page charges. This article must therefore be hereby marked "advertisement" in accordance with 18 U.S.C. Section 1734 solely to indicate this fact.

[‡] To whom correspondence should be addressed: Dept. of Plant Biology, Michigan State University, Wilson Dr., East Lansing, MI 48824-1312. Tel.: 517-355-5237; Fax: 517-353-1926; E-mail: Schwend2@msu.edu.

¹ The abbreviations used are: OPPP, oxidative pentose phosphate pathway; C18, octadecanoic acid; C18:1, octadecenoic acid; C22, eicosanoic acid; C22:1, docosenoic acid; DHAP, dihydroxyacetone phosphate; Fru-6-P, fructose 6-phosphate; GAP, glyceraldehyde 3-phosphate; Glc-6-P, glucose 6-phosphate; GC, gas chromatography; MS, mass spectrometry; PEP, phosphoenol pyruvate; Rib-5-P, ribose-5-phosphate; Ru-5-P, ribulose 5-phosphate; Suc, sucrose; TAG, triacylglycerol; TA, transaldolase; TK, transketolase; Xu-5-P, xylulose 5-phosphate; PDH, pyruvate dehydrogenase complex.

and end-products of metabolism can provide information on the relative fluxes through alternative pathways and on flux ratios at branch points between pathways (see, for example, Refs. 35–37). With *in vivo* labeling, this approach yields quantitative information on systems unperturbed by cell disruption, mutations, or transgenic manipulation. The results of this approach can therefore distinguish the relative contributions of competing pathways and help guide rational engineering of metabolism.

To take advantage of such methods, we have recently established culture conditions for developing *B. napus* embryos that mimic *in planta* growth and allow steady state labeling during storage product accumulation (22). After feeding ^{13}C -labeled carbon sources, the labeling pattern of various intermediates of central carbon metabolism are “imprinted” on seed oil and on the amino acids of seed protein; these can be measured by gas chromatography/mass spectrometry (GC/MS) and by NMR spectroscopy. Using these techniques, we deduced that the pyruvate that provides acetyl-CoA units for fatty acid is derived from Glc almost entirely by glycolytic cleavage (Embden-Meyerhof pathway) and that glycolysis rather than the OPPP accounts for most embryo hexose catabolism. Based on a preliminary analysis of labeling in fatty acids, we estimated that the net flux of Glc-6-P into OPPP is in the range of 5–10% of total influx of Glc-6-P. However, this preliminary estimate was based on making key assumptions about the reversibilities of transketolase (TK; EC 2.2.1.1) and transaldolase (TA; EC 2.2.1.2). In the present study, we have developed a quantitative model of glycolysis and OPPP and tested its ability to account for isotopomer labeling patterns and to yield reliable flux parameters in developing *B. napus* seeds.

EXPERIMENTAL PROCEDURES

Chemicals—[U- $^{13}\text{C}_6$]Glc, [1,2- $^{13}\text{C}_2$]Glc, [1- ^{13}C]Glc, [6- ^{13}C]Glc, and [2- ^{13}C]Glc (all 99% ^{13}C abundance) were purchased from Isotec (Miamisburg, OH) and Omicron (South Bend, IN). Methoxyamine hydrochloride, α -amylase (EC 3.2.1.1) and *Aspergillus niger* amyloglucosidase (EC 3.2.1.3) were purchased from Sigma.

Growth in the Presence of ^{13}C -Labeled Sugars—Oilseed rape plants (*B. napus* L., cv. Reston) were grown as described before (22). Siliques were harvested 20 days after flowering, and embryos were immediately dissected under aseptic conditions and transferred into culture medium (22). In order to obtain fully labeled TAG and seed protein for analysis by GC/MS, five embryos were isolated at the early stage of oil accumulation (0.5–1 mg of fresh weight) and were grown for 14 days, each in 5 ml of growth medium under low light conditions (continuous light, 50 $\mu\text{mol m}^{-2} \text{s}^{-1}$) under aseptic conditions. The growth medium contained Suc (80 mM), Glc (40 mM) and amino acids as carbon sources in concentrations that closely mimic *in planta* conditions during maximal oil synthesis (22). For different labeling experiments, part of the Glc or Suc was replaced by ^{13}C -labeled sugars. A 1:10 isotopic dilution of ^{13}C -labeled Glc was achieved by a mixture of, for example, [1,2- $^{13}\text{C}_2$]Glc/Glc/Suc (10:10:80) (mol % hexose units) or, in the case of uniformly ^{13}C -labeled sugars, by a mixture of [U- $^{13}\text{C}_6$]Glc/Glc/[U- $^{13}\text{C}_{12}$]Suc/Suc (2:18:8:72) (mol % hexose units). Experiments with Glc labeled in different positions were also performed using, for example, [1- ^{13}C]Glc/[1,2- $^{13}\text{C}_2$]Glc/Suc (10:10:80) (mol % hexose units).

In some experiments aimed at analysis of intermediates and starch, embryos were labeled for 3 days. In one such experiment, embryos were cultured with [U- $^{13}\text{C}_6$]Glc/Glc/[U- $^{13}\text{C}_{12}$]Suc/Suc (2:18:8:72) (mol % hexose units), and after 3 days labeled Suc, free amino acids, and starch were extracted and analyzed by GC/MS methods. In other experiments aimed at labeling free Suc and starch, 50 embryos in the early stage of oil accumulation (2–3 mg fresh weight) were grown for 3 days in 20 ml of growth medium with either [1- ^{13}C]Glc or [6- ^{13}C]Glc (99% ^{13}C enrichment, 20 mM). Since Suc labeled at C-1 or C-6 of hexose units was not available, Suc in the growth medium was substituted by its analog palatinose (6-*O*- α -D-glucopyranosyl-D-fructofuranose, 80 mM), which is not taken up or metabolized in plants but which appears to have similar signal functions to Suc (38). Therefore, in these experiments, the main carbohydrate carbon source was the labeled Glc, and the starch and seed oil in the embryos were substantially labeled. These experiments yielded 1–10 mg of free Suc, Glc (from starch), and seed oil for analysis

by NMR spectroscopy. To ensure that the palatinose in the growth medium has no major artificial influence on the results, analogous experiments using [1- ^{13}C]Glc with unlabeled sucrose were also performed, which confirmed the experimental results with palatinose although with inferior accuracy due to the isotopic dilution of label from the unlabeled sucrose.

Extraction of Lipids and Proteins—Labeled embryos were ground, and lipids were extracted with hexane/diethylether (1:1, v/v); proteins were extracted in a buffer containing sodium phosphate, pH 7.5 (10 mM), and NaCl (500 mM) as described by Schwender and Ohlrogge (22). Extracted soluble proteins were precipitated by the addition of one-tenth volume of 50% trichloroacetic acid.

Extraction of Sucrose—Embryos labeled for 3 days were ground in a glass homogenizer in methanol/H₂O (1:1) (v/v) and extracted three times at 50 °C. The combined extracts were separated into a water-soluble and a lipid fraction by adding chloroform to a final ratio close to CHCl₃/methanol/H₂O (8:4:3) (39). The aqueous phase containing mainly Suc was freeze-dried and dissolved in D₂O for NMR analysis.

Starch Degradation—After extraction of lipids and water/methanol-soluble compounds, the cell residue (equivalent to 50–100 mg fresh weight tissue) was washed three times with 5 ml of 80% (v/v) aqueous methanol and dried under vacuum. After the addition of 1 ml of H₂O and sealing and heating at 110 °C for 1 h, starch was degraded to Glc by the addition of 1 ml of 0.1 M acetate buffer (pH 4.8), 20 units α -amylase, and 20 units amyloglucosidase with heating to 55 °C for 3 h. Proteins were precipitated by the addition of 1 volume of ethanol, sealing and heating to 100 °C for 5 min, and centrifugation. The supernatant was reduced in volume by evaporation under nitrogen, freeze-dried, and dissolved in D₂O for ^{13}C NMR spectroscopy or derivatized for GC/MS analysis.

Measurement of Glucose Labeling—For analysis by GC/MS, Glc was derivatized to Glc methoxime penta-acetate. 1 ml of methoxyamine hydrochloride in pyridine (20 mg/ml) was added to 50–100 μg of Glc and heated to 50 °C for 1 h. After cooling to room temperature, 1 ml of acetic acid anhydride was added, and the sample was again heated to 50 °C for 1 h. Finally, the derivative was extracted with toluene after adding 1 volume of H₂O to the reaction. The ions *m/z* 360, *m/z* 289, and *m/z* 89 (C₁₆H₂₂O₉N (Glc_(1–6)),² C₁₂H₁₇O₉N (Glc_(3–6)), and C₃H₇O₂N (Glc_(1–2)), respectively) were monitored by GC/MS.

Measurement of Lipid Labeling—For analysis by GC/MS or ^{13}C NMR, the lipid fraction consisting mainly of TAG was hydrogenated (40). For analysis of fatty acids and glycerol by GC/MS, lipids were transesterified by heating to 90 °C in 5% (w/v) HCl in methanol for 1 h. After cooling to room temperature, 1 volume of H₂O was added, and fatty acid methyl esters were extracted with hexane (41). The aqueous phase was freeze-dried, and the residue, containing glycerol, was derivatized with trifluoroacetic acid anhydride for 1 h at room temperature to obtain glycerol trifluoroacetate. Residual derivatization reagent was removed with a stream of nitrogen, and the derivatives were dissolved in toluene.

Measurement of Label in Amino Acids of Storage Proteins—Proteins were hydrolyzed in 6 N HCl for 24 h at 100 °C. HCl was evaporated at 50 °C under a stream of nitrogen. Amino acids were dissolved in 0.1 N HCl and loaded on an H⁺ exchange column (AG 50W-X4; Bio-Rad). After washing with 5 volumes of H₂O, amino acids were eluted with 2 N NH₄OH. After most of the NH₄OH was removed under a stream of nitrogen, the sample was lyophilized and then derivatized to their *N,O*-tert-butylidimethylsilyl derivatives by adding 100 μl of *N*-methyl-*N*-(tert-butylidimethylsilyl)-trifluoroacetamide/acetonitrile (1:1) to 100 μg of amino acids and heating at 120 °C for 1 h (36, 42). The identities of different fragments of the TBDMS amino acid derivatives in mass spectra were derived from the literature (36, 42).

GC Conditions—One microliter of each derivatized sample (100–500 ng/ μl) was analyzed with a HP 5890 II (Hewlett-Packard) gas chromatograph/mass spectrometer (HP 5972 quadrupole MS). Carrier gas was helium at 1 ml/min. For fatty acid methyl esters, a DB23 column (30 m \times 0.25 mm) was used (J&W Scientific, Folsom, CA). For *N,O*-tert-butylidimethylsilyl derivatives of amino acids, Glc methoxime penta-acetate, and glycerol trifluoroacetate, a 30 m \times 0.25-mm DB1 column was used (J&W Scientific). The GC conditions for fatty acid methyl esters and *N,O*-(*S*)-tert-butylidimethylsilyl derivatives of amino acids were as previously described (22). For glycerol trifluoroacetate, the injector temperature was 250 °C. Initial temperature was 60 °C for

² Carbon atoms in different molecules are denoted as subscripts. For example, Glc_(1–3) refers to the part of the molecule comprising carbons 1, 2, and 3 of Glc, and pyruvate_(1–2) refers to carbons 1 and 2 of pyruvate.

2 min, increased to 240 °C at 20 °C/min and a final temperature at 240 °C for 10 min. Data were analyzed by the Chem Station Program (HP G1043C, Hewlett-Packard).

Measurement of Fractional Labeling by Mass Spectrometry—In mass spectra of labeled compounds, selected molecular fragments were monitored. Single ion monitoring was generally used with >20-ms acquisition time for each ion. The mass spectra of each ion were integrated over the entire chromatographic peak to avoid the influence of possible isotope fractionation during GC separation. Background correction was performed with mass spectra taken just before each chromatographic peak. Reproducibility of isotope ratios was checked with unlabeled reference substances over a concentration range of 2 orders of magnitude. The ion clusters were corrected for natural isotope abundance in heteroatoms and in derivative residues as well as in the labeled molecule (43). The molar abundances of molecule fragments containing *i* labeled carbons are referred to as m_i . The identity of ions was checked by comparison of the measured mass distribution of a fragment of unlabeled compounds with the theoretical distribution, as derived from the elemental composition and natural isotope abundances (43). Only fragments that were in good agreement with the theoretical mass distribution were used for measurements. In the case of TBDMS-amino acids and Glc methoxime penta-acetate, the ion purity was also verified by derivatization of ¹³C-labeled amino acids (hydrolysis of U-¹³C-labeled protein, 99% ¹³C; Isotec) and Glc ([1-¹³C]Glc, [6-¹³C]Glc, [1,2-¹³C₂]Glc, and [U-¹³C₆]Glc), respectively, which leads to mass shifts of the isotopomer clusters defined by the presence of one or more ¹³C-labeled carbon atoms in the monitored fragment. The fragmentation of glycerol trifluoroacetate during MS analysis was established by analogy to glycerol triacetate (44). The fragment *m/z* 158 contains glycerol₍₁₋₃₎. In the mass spectra of saturated fatty acid methyl esters, the ion *m/z* 74 can be used to measured labeling in C18₍₁₋₂₎ (22). Since in the extracted TAG, C18:1 dominated over C18 and since fatty acids were hydrogenated before GC/MS analysis, the measured C18₍₁₋₂₎ represents mainly C18:1₍₁₋₂₎.

Comparison of Measured and Simulated Labeling in Glucose by Least Squares Fitting—Embryos were labeled for 14 days with [U-¹³C₁₂]Suc/[U-¹³C₆]Glc (each diluted 1:10 with unlabeled sugar). Labeling in the glucosyl units of starch was measured by GC/MS. The fractional ¹³C enrichment was measured in the fragments Glc₍₁₋₂₎, Glc₍₃₋₆₎, and Glc₍₁₋₆₎. The measured mass isotopomers³ m_1 and m_2 of Glc₍₁₋₂₎, m_1 to m_4 of Glc₍₃₋₆₎, and m_1 to m_6 of Glc₍₁₋₆₎ were compared with values predicted by the computer model. For each mass isotopomer *i*, the difference between measurement and prediction (Δ_i) was calculated. The sum of squared differences ($\Sigma\Delta_i^2$) was calculated as a measure for the similarity between measured and predicted mass isotopomers. By variation of the model parameters X , V_{TK} , V_{TA} , and V_{TPC} , minima for $\Sigma\Delta_i^2$ were determined as shown in Figs. 3 and 4.

NMR Analysis—NMR analyses of aqueous extracts (containing predominantly Suc) of Glc (isolated from starch) and of storage lipids (mainly triacylglycerols) were performed with a Varian VXR 500 MHz spectrometer equipped with a 5-mm ¹³C-¹H switchable probe. ¹H and ¹³C NMR spectra were measured with a 90° pulse angle, ¹H waltz decoupling during acquisition only (for ¹³C spectra), and full relaxation (recycle times = 60 s). Data processing included zero filling and multiplication of the free induction decays by an exponential function to improve the signal-to-noise ratio. NMR peak assignment for Glc, Suc, and TAG was performed using literature values (45) and by comparison with pure reference substances. The absolute ¹³C enrichment in Suc and Glc was determined by ¹H NMR of Suc glucosyl C-1 and α -C-1 of Glc, respectively. In addition, absolute ¹³C enrichment was determined by GC/MS of methoxyamine penta-acetates of Glc.

THEORY

Defining the Metabolic Network

The crucial first stage in building quantitative models of metabolic flux is constructing a map of the metabolic network to be analyzed. Such a scheme for the principal flows of carbon into protein, starch, and oil in developing *B. napus* embryos is shown in Fig. 1. This map is the basis for the quantitative modeling of fluxes described below, and it is based on the biochemical literature including enzyme localization *in vitro* and *in vivo* labeling studies. Since *Brassica* and *Arabidopsis*

thaliana are considered to have very similar genomes and seed metabolism, recent transcriptional profiling of developing *Arabidopsis* seeds (46) and information from the *Arabidopsis* genome were also used to construct the network shown in Fig. 1. Key features of the metabolic network illustrated in Fig. 1 are described below.

Sugar Catabolism—During oil accumulation, *B. napus* embryos use Suc, as well as Glc and fructose, as carbon sources for fatty acid synthesis (12, 22, 23). Suc is mostly cleaved by Suc synthase (EC 2.4.1.13) (12, 23). The cleavage products are metabolized through glycolysis, the enzyme activities of which are present in both cytosol and plastid (3, 9, 14). Resynthesis of Fru-6-P from triose phosphate is possible by plastidic fructose-1,6-bisphosphatase (EC 3.1.3.11) or cytosolic pyrophosphate-dependent fructose-6-phosphate-1-phosphotransferase (EC 2.7.1.90) (9). Exchange of intermediates between cytosol and plastids can occur by the transport of Glc-6-P, triose phosphate, PEP, pentose phosphate, and pyruvate (3, 9, 14, 46).

Starch Metabolism—In developing *B. napus* seeds, starch is accumulated inside the chloroplasts mainly before the main stage of oil accumulation but is still present at later stages and is continuously turned over (5). Therefore, the labeling in starch can be assumed to represent the plastidial hexose phosphate during maximal oil deposition. For *B. napus* embryos, it was concluded that hexose is mainly imported into the plastids in the form of Glc-6-P, whereas Glc-1-P was not used by isolated plastids (9). Import of the starch precursor ADP-Glc into the plastids can be excluded because of the subcellular localization of ADP-Glc pyrophosphorylase (EC 2.7.7.27) in *B. napus* embryos (5, 14, 47).

Incomplete Cytosolic OPPP—In developing *B. napus* seeds, glucose-6-phosphate dehydrogenase (EC 1.1.1.49) activity is found in plastids and the cytosol (9, 14). The regeneration of Fru-6-P from pentose phosphate involves ribose-5-phosphate isomerase (EC 5.1.3.1), ribulose-5-phosphate epimerase (EC 5.3.1.6), TK, and TA. In *Arabidopsis*, there are most probably only plastidic isoforms of TK and TA (48). Similar results for spinach leaves (49) and other tissues (50) also point to an incomplete OPPP in the cytosol. Therefore, cytosolic regeneration of Fru-6-P from pentose-phosphate by TK and TA were not included in the network. Instead, it was assumed that pentose phosphate, if produced in the cytosol, can be transported into the plastid by a pentose phosphate-specific transporter (48).

Transport of Carbon into Plastids—Import of carbon into isolated plastids of developing *B. napus* embryos has been reported for many substrates including Glc-6-P, DHAP, malate, pyruvate, PEP, and free hexoses (9). Evidence for Glc-6-P, PEP, and triose phosphate transporters also comes from transcription profiling of developing seeds of *A. thaliana* (46). During maximal oil synthesis, it has been proposed that the main flux of carbon enters the chloroplasts as PEP or pyruvate with a minor influx of Glc-6-P (3, 46, 51). This is supported by isotopic tracer experiments with isolated plastids and by the change of plastidial activities of enzymes of glycolysis during embryo development (2, 3, 8, 9). Furthermore, in developing embryos of *A. thaliana*, the expression of the PEP translocator follows the pattern of enzymes involved in oil synthesis (plastidic pyruvate kinase (EC 2.7.1.40) and plastidic pyruvate dehydrogenase (E1a)), peaking with maximal oil synthesis, whereas the expression of cytosolic pyruvate kinase decreases with the onset of oil synthesis (46). Therefore, Fig. 1 includes a major carbon influx into the plastid at the level of PEP, although the *in vivo* contribution of other transport processes cannot be ruled out.

Plastidic Fatty Acid Synthesis and Cytosolic Elongation—In plant systems, fatty acid synthesis is localized predominantly

³ The molar abundances of molecule fragments containing *i* labeled carbons are referred to as m_i .

phosphates Xu-5-P, Ru-5-P, and Rib-5-P, which interconvert via ribulose-5-phosphate-3-epimerase (EC 5.3.1.6) and ribose-5-phosphate isomerase (EC 5.1.3.1), respectively, are also treated as one pool (PP; Fig. 2). A rapid exchange between Xu-5-P and Rib-5-P (via Ru-5-P), relative to the flux through oxidative decarboxylation of Glc-6-P, is supported by the observation of a TK signature in histidine (see "Results").

Fluxes of Glucose 6-Phosphate, Pentose Phosphate, and Erythrose 4-Phosphate into Cell Wall Polymers and Protein—Mature *B. napus* embryos contain ~50% oil, 30% protein, 8% water, and 7% sugars and cell wall polymers (67). From this, it can be estimated that at most 5% of the total Glc influx is used for cell wall synthesis. The seed protein consists of 60% (w/w) cruciferin, 20% (w/w) napin, and 20% (w/w) oleosin (68). Based on the fraction of His, Trp, Phe, and Tyr in seed protein (68, 69), the flux of pentose phosphate into His and Trp is about 0.6% of the total Glc influx, and the flux of erythrose 4-phosphate into Phe, Tyr, and Trp is about 1% of the total Glc influx. These small fluxes into cell wall polymers and into Phe, Tyr, Trp, and His were not included in the model (Fig. 2).

Defining the Proportion of Glucose Metabolized via the OPPP and the Reversible Fluxes—In the OPPP Glc-6-P is oxidized to pentose phosphate and CO₂, with production of 2 NADPH/mol

of Glc-6-P oxidized (Fig. 2). A cyclic flux is established by regeneration of Fru-6-P from pentose phosphate and by the isomerization of Fru-6-P to Glc-6-P. In the first flux model for glycolysis and OPPP, Katz and Wood (70) defined the flux parameter *X* for the proportion of Glc-6-P that is "degraded to smaller units" (i.e. into CO₂ and triose phosphate) by the action of the OPPP. Thus, *X* defines the split of *net* Glc utilization between glycolysis and OPPP as being 1 - *X* and *X*, respectively (Table I). According to this convention, the flux through Glc-6-P DH is 3*X* (Table I), although in some studies (e.g. Ref. 31), the OPPP flux is defined as the total molar flux through Glc-6-P DH, which corresponds to 3*X* in our notation. The reversibility fluxes (fluxes in both forward and reverse directions that act in addition to the net fluxes) at TK, at TA, and between hexose P and triose phosphate are designated *V*_{TK}, *V*_{TA}, and *V*_{TPC}, respectively (Table I). These three model parameters together with *X* were determined by a recursive fitting procedure that minimizes the sum of squared differences between measured and simulated labeling levels in metabolites ($\Sigma\Delta^2$).

Computer Program—We developed a computer program (Microsoft Visual Basic/Excel™ Macro Language), which can predict the steady state distribution of ¹³C-labeled Glc in the glycolysis/OPPP network (see Appendix). It has an interface with an Excel™ spreadsheet for input of parameters and for the output of calculated steady state isotopomer enrichments in metabolite pools (hexose 6-phosphate, pentose 5-phosphate, sedoheptulose 7-phosphate, erythrose 4-phosphate, triose phosphate, and acetyl-CoA). The program also calculates positional enrichments (percentage of ¹³C at each carbon position) for comparison with NMR spectra and the abundances of mass isotopomers for simulating mass spectra. Labeling experiments with singly ¹³C-labeled sugars as well as [1,2-¹³C₂]Glc or [U-¹³C₆]Glc or mixtures of labeled and/or unlabeled sugars can be simulated. Input parameters required by the simulation program are the relative flux rates (*X*, *V*_{TK}, *V*_{TA}, and *V*_{TPC}; see Fig. 2) and the labeling levels of the supplied Glc. The software is available from the authors on request.

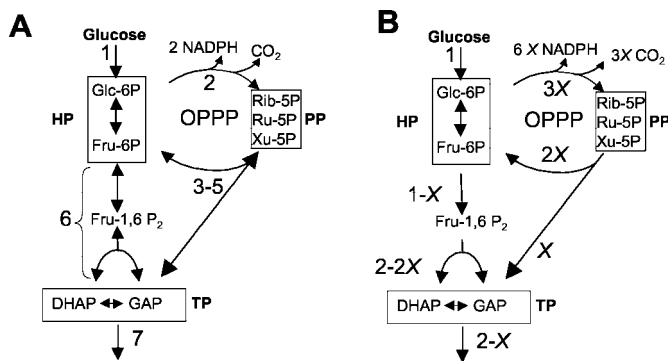


FIG. 2. Illustrations of the flux model for carbon flux in the glycolysis/OPPP network. Three groups of metabolically adjacent metabolites are considered to be in isotopic equilibrium with one another, and these groups are treated as single metabolic pools in the model. These are shown in boxes: hexose phosphate (HP), pentose phosphate (PP), and triose phosphate (TP). A shows the reactions modeled: 1, hexokinase; 2, glucose-6-phosphate dehydrogenase and phosphogluconate dehydrogenase; 3, transketolase; 4, transketolase; 5, transaldolase; 6, phosphofructokinase and aldolase. The reaction numbers are the same as in Table I. B shows the net fluxes through each of these reactions relative to the rate of uptake of Glc which is defined as 1. The forward, reverse, and net fluxes for these reactions are listed in Table I.

TABLE I

Steady state equations of the reactions of the network glycolysis/OPPP (see also Fig. 2)

Reactions with net fluxes and definition of forward and reverse fluxes are shown. Reaction 1 represents the carbon influx into the system, which is normalized to 1. Reactions 2–5 add up to reaction 6, which is the net flux through OPPP and which has a rate of *X*. Note that the net flux through Glc-6-P oxidation (reaction 2) is 3*X*. Since the influx of Glc into the system is 1 and Glc-6-P is degraded via OPPP with the rate *X*, the rate of glycolytic degradation of Fru-6-P is 1 - *X* (reaction 7). Thus, *X* describes the split of carbon flux between OPPP and glycolysis. Reactions are as follows (see Fig. 2): 1, hexokinase; 2, glucose-6-phosphate dehydrogenase and phosphogluconate dehydrogenase; 3, transketolase 1; 4, transketolase 2; 5, transaldolase; 6, sum of OPPP reactions; 7, phosphofructokinase/aldolase; 8, glyceraldehyde-3-phosphate dehydrogenase. E-4-P, erythrose 4-phosphate; Sh-7-P, sedoheptulose 7-phosphate.

Reaction	Reaction	Net flux	Forward rate	Reverse rate
1	Glc → Glc-6-P	1	1	0
2	Glc-6-P → Ru-5-P + CO ₂	3 <i>X</i>	3 <i>X</i>	0
3(TK ₁)	Rib-5-P + Xu-5-P → Sh-7-P + GAP	<i>X</i>	<i>X</i> + <i>V</i> _{TK}	<i>V</i> _{TK}
4(TK ₂)	E-4-P + Xu-5-P → Fru-6-P + GAP	<i>X</i>	<i>X</i> + <i>V</i> _{TK}	<i>V</i> _{TK}
5	Sh-7-P + GAP → E-4-P + Fru-6-P	<i>X</i>	<i>X</i> + <i>V</i> _{TA}	<i>V</i> _{TA}
6	Glc-6-P → GAP + 3CO ₂	<i>X</i>		
7	Fru-6-P → DHAP + GAP	1 - <i>X</i>	1 - <i>X</i> + <i>V</i> _{TPC}	<i>V</i> _{TPC}
8	GAP → PGA	2 - <i>X</i>		

TABLE II
Randomization of ^{13}C label between the upper and lower three carbons in starch (glucose) and in the glucosyl and fructosyl moieties of sucrose from labeled embryos

Embryos were grown for 3 days on $[1-^{13}\text{C}]\text{Glc}$ or $[6-^{13}\text{C}]\text{Glc}$. In order to obtain maximal ^{13}C label in Suc and starch, Suc was substituted by palatinose, which is not metabolized (see "Experimental Procedures"). ^{13}C label in C-1 and C-6 of hexose units was determined by ^{13}C NMR. Using the ratio C-1/C-6, the flux parameter for reversible interconversion of triose phosphate and Fru-6-P (V_{TPC}) was determined assuming $X = 0.12$, $V_{\text{TA}} = 0.01$, and $V_{\text{TK}} = 0.95$. X , V_{TA} , and V_{TK} were obtained by other labeling experiments (see "Metabolic Fluxes"). By simulation with different values for V_{TPC} , X , V_{TA} , and V_{TK} , it was found that V_{TPC} is well determined by the ratio C-1/C-6 and largely independent from the values for X , V_{TA} , and V_{TK} in particular for the labeling with $[6-^{13}\text{C}]\text{Glc}$. Confidence intervals are given based on $\pm 1\%$ error in measured ^{13}C contents of C-1 and C-6.

Precursor	Metabolite analyzed	Measured C-1/C-6 ratio	V_{TPC} fitted to C-1/C-6 ratio
$[1-^{13}\text{C}]\text{Glc}/\text{Palatinose}$	Suc glucosyl	2.7 (2.6–2.9)	1.0 (0.9–1.1)
	Suc fructosyl	2.3 (2.2–2.5)	1.4 (1.3–1.5)
	Starch glucosyl	2.4 (2.3–2.5)	1.3 (1.2–1.5)
$[6-^{13}\text{C}]\text{Glc}/\text{Palatinose}$	Suc glucosyl	0.20 (0.19–0.21)	0.6 (0.5–0.7)
	Suc fructosyl	0.23 (0.22–0.25)	0.8 (0.7–0.9)
	Starch glucosyl	0.25 (0.23–0.27)	0.8 (0.7–0.9)

TABLE III
Comparison of the measured and simulated m_1/m_2 ratios for different metabolites

The m_1/m_2 ratio was measured by GC/MS in different metabolites after labeling with $[1,2-^{13}\text{C}_2]\text{Glc}$ or with mixtures of $[1,2-^{13}\text{C}_2]\text{Glc}$ with $[1-^{13}\text{C}]\text{Glc}$ or with $[6-^{13}\text{C}]\text{Glc}$. Observed values (Obs.) are compared with values simulated (Sim.) using the parameters $X = 0.12$; $V_{\text{TA}} = 0.01$; $V_{\text{TK}} = 0.95$; $V_{\text{TPC}} = 1.0$ (10% enrichment of the supplied Glc). In each experiment, 3–5 embryos were grown separately, each in 5 ml of medium. The embryos were extracted, and the experimental value of m_1/m_2 is an average of three GC/MS measurements with S.D. $< 2.5\%$ (for C18:1 $_{(1-2)}$). For the experiments with a $1-^{13}\text{C}/1,2-^{13}\text{C}_2$ ratio of 1:1, the values represent the average of triplication of the experiment, resulting in S.D. values of 2–8% of m_1/m_2 . *pl.*, plastidic; *cyt.*, cytosolic.

Fragment	Precursor	Labeled substrate supplied (Glc)					
		$1,2-^{13}\text{C}_2$		$1,2-^{13}\text{C}_2/1-^{13}\text{C} = 1:1$		$1,2-^{13}\text{C}_2/6-^{13}\text{C} = 1:1$	
		Obs.	Sim.	Obs.	Sim.	Obs.	Sim.
Gluc $_{(1-2)}$ of starch	<i>pl.</i> Glc-6-P $_{(1-2)}$	ND ^a		1.16	1.24	0.38	0.58
Ala $_{(1-3)}$	Pyruvate $_{(1-3)}$	0.46	0.38	1.50	1.45	1.76	1.65
Glycerol $_{(1-3)}$	<i>cyt.</i> DHAP $_{(1-3)}$	ND		1.31	1.45	ND	
Ala $_{(2-3)}$	Pyruvate $_{(2-3)}$	0.28	0.22	1.21	1.24	1.54	1.47
Val $_{(2-5)}$ ^b	2× pyruvate $_{(2-3)}$	0.25	0.22	1.21	1.24	1.42	1.47
C18:1 $_{(1-2)}$	<i>pl.</i> acetyl-CoA $_{(1-2)}$	0.21	0.22	1.24	1.24	1.48	1.47
His $_{(1-6)}$	<i>pl.</i> pentose-P $_{(1-5)}$	0.43	0.54	1.48	1.55	1.40	1.39

^a ND, not determined.

^b Val $_{(2-5)}$ represents a fragment generated by the loss of C-1 of valine. The resulting 4-carbon fragment consists biosynthetically of two units of pyruvate $_{(2-3)}$. To calculate the m_1/m_2 ratio in pyruvate $_{(2-3)}$ from the labeling data of Val $_{(2-5)}$, probabilistic equations were used that describe the mass spectrum of a fragment formed by two identically labeled fragments from pyruvate $_{(2-3)}$.

Model Validation

If a steady state flux model of metabolism of this type is to be useful, several criteria must be met; its underlying assumptions need to be tested, its results should be consistent and reproducible, and the flux parameters derived should be sensitive to the labeling data used. We examined these criteria as follows.

Isotopic Steady State and Metabolic Homogeneity—To establish steady state, nutrient concentrations were kept constant during growth of embryos in culture by providing nutrients in more than 10-fold surplus to the expected uptake during the growth period. The concentrations of sugars in growth media were measured after 14 days of growth and found to be only minimally altered (data not shown). Embryos were grown for 3 days and for 14 days on $[\text{U}-^{13}\text{C}_6]\text{Glc}/[\text{U}-^{13}\text{C}_{12}]\text{sucrose}$. During the 14-day culture period, the biomass increased more than 10-fold. With a 3-day labeling period, it was found by GC/MS analysis that about one-third of the fatty acid molecules of seed oil were labeled, whereas two-thirds were unlabeled preexisting biomass, whereas after 14 days, the oil was uniformly labeled. By contrast, the labeling pattern in sucrose, free amino acids, and starch was the same after 3 days as after 14 days of labeling. From this it can be concluded that there is the same fractional labeling in intermediate metabolic pools after 3 days and after 14 days, which indicates that both metabolic and isotopic labeling steady state were maintained during the experimental growth period and that metabolic pools that are

turned over (sucrose, free amino acids, and starch) can be used for analysis under the steady state assumption after labeling for shorter periods.

Equilibration of DHAP and GAP—Whereas fatty acids are derived from pyruvate and hence from plastidic GAP, the glycerol part of TAG molecules is derived from cytosolic DHAP (Fig. 1). Thus, measuring labeling in glycerol and fatty acids allows a comparison of DHAP and GAP pools. Labeling was analyzed in TAG extracted from embryos that had been labeled with $[1-^{13}\text{C}]\text{Glc}$, $[6-^{13}\text{C}]\text{Glc}$, or $[1,2-^{13}\text{C}_2]\text{Glc}$, and the findings indicated that in both cytosol and plastids, the pools of GAP and DHAP are isotopically equilibrated (data not shown). Accordingly, the flux model unifies DHAP and GAP as one triose phosphate pool (Fig. 2).

Interconversion of Hexose Phosphates—Synthesis of Fru-6-P from triose phosphate causes the exchange of ^{13}C label between C-1 and C-6 in Fru-6-P (Table II). To the extent that Glc-6-phosphate isomerase (EC 5.3.1.9) interconverts Fru-6-P and Glc-6-P, this exchange can also be found in Glc 6-P. We measured the extent of randomization of label between C-1 and C-6 in Glc derived from starch and in both hexose moieties of sucrose (Table II). The same degree of C-1/C-6 randomization was seen in both hexose moieties of sucrose, indicating that cytosolic glucose-6-phosphate isomerase equilibrates the Glc-6-P and Fru-6-P pools rapidly compared with the other fluxes of the network being modeled. The same C-1/C-6 randomization was also found in starch (Table II), suggesting that the plastidic and cytosolic pools of hexose phosphates have the same

metabolic imprints. In the flux model, the hexose phosphate pools were treated as one pool.

Consistency and Reproducibility of Modeling Results—Consistency of modeling results is tested in three ways. To test for internal consistency, data output is automatically tested for steady state (summation of influx and efflux into each isotope = 0) and for conservation of mass (sum of all isotopes in one pool = 1). Also, arithmetic instability was considered as described in Ref. 66. Second, we tested the modeling results for consistency with the results of equations systems that have been solved analytically elsewhere. Data output from the model using different sets of values for X , V_{TA} , and V_{TK} was compared with the output of steady state equation systems developed by Katz and Rognstad (71). The Katz and Rognstad equations allow the distribution of label in a subset of metabolic pools (hexose phosphate, pentose phosphate, and sedoheptulose 7-phosphate) to be calculated after labeling with either $[1-^{14}C]Glc$, $[2-^{14}C]Glc$, or $[6-^{14}C]Glc$ (assuming $V_{TPC} = 0$). In addition, output data of our computer model matched data produced by a steady state equation system from Follstad and Stephanopoulos (65), which yields positional labeling in certain metabolites. Third, the values of flux parameters obtained by fitting the labeling patterns measured in one metabolite were checked for consistency with the label in another metabolite. For example, the value of X (glycolysis/OPPP split) obtained from analysis of fatty acids (m_1/m_2 ratio) was found to also explain the observed labeling in Ala, Val, His, and Glc (starch) (Table III).

Reproducibility of modeling results depends on the variation in labeling data both when the same sample is analyzed repeatedly and when different replicate experiments are performed. In general, reproducibility of repeated GC/MS analyses of the same sample was higher than that of replicate experiments. Repeated measurements of m_1/m_2 ratios resulted in S.D. values of <2.5%, whereas triplication of experiments resulted in S.D. values between 2 and 8% of m_1/m_2 (Table III). In the data shown in Table III, reproducibility is also given by comparison of experiments with differently labeled substrates. Based on the flux model, the same value for X explains data from labeling with $[1,2-^{13}C_2]Glc$, $[1,2-^{13}C_2]Glc/[1-^{13}C]Glc$, and $[1,2-^{13}C_2]Glc/[6-^{13}C]Glc$ (Table III). Due to the cost and time involved in stable isotope labeling experiments, achieving replication is a nontrivial matter and is less often done than is desirable. In this study, we have in some cases triplicate reproduction of experimental results, and in addition, by performing a number of the experiments with similar substrates as described in Table III, we have achieved additional cross-checks on our conclusions.

Sensitivity of Model Parameters to Variation in Labeling Experiments—After embryos were cultured for 14 days with $[U-^{13}C_{12}]sucrose/[U-^{13}C_6]Glc$, the labeling of Glc was measured by GC/MS in three fragments of Glc. Figs. 3 and 4 illustrate the fitting of model parameters to measured data. Fitting was performed by minimizing the sum of squared differences ($\sum \Delta_i^2$) between measured and simulated labeling patterns (see "Experimental Procedures"). For statistical analysis, a threshold of significance for the fitting results was defined to reflect the level of uncertainty introduced into the derived flux parameter values by the uncertainty in the experimental data. This threshold for the value of $\sum \Delta_i^2$ was conservatively set at 100 times the sum of the squared S.D. values of the experimental data (replicate measurements of the same experimental material). This yields confidence limits for the flux parameters (Figs. 3 and 4, Table IV).

Figs. 3 and 4 show that there are clear optima for fitting V_{TK} , V_{TA} , and V_{TPC} to experimental data and that the model param-

eters are sensitive to the experimental data, since changes in any optimized parameter value lead to a significantly worse fitting of model results to measured data. By comparing the shapes of the curves shown in Fig. 3, A and B, one can see that the slopes at the left and the right side of the optima are similar for V_{TPC} and V_{TK} . This means that the sensitivity of both flux parameters is similar. The optimum for V_{TA} is close to 0 (Fig. 4B). With increasing V_{TA} , the slope is similar to that found with V_{TPC} and V_{TK} (not shown).

After labeling with $[1,2-^{13}C_2]Glc/[1-^{13}C]Glc$, the ratio m_1/m_2 was determined for three independent experiments. The S.D. of these experimental data translates according to the flux model to an S.D. in the derived value of X (Fig. 5). Since the two standard deviations in m_1/m_2 and X are similar, the flux X can be described as "well determined" (72).

Metabolic Fluxes

Interconversion of Fru-6-P and Triose Phosphate—When embryos were labeled with either $[1-^{13}C]Glc$ or $[6-^{13}C]Glc$ for 3 days, the hexose units of sucrose and of starch all showed substantial randomization of label between C-1 and C-6 (Table II), indicative of triose phosphate cycling. By simulation, values for V_{TPC} between 0.6 and 1.4 were found (Table II). In other experiments, embryos were labeled with $[U-^{13}C_{12}]sucrose/[U-^{13}C_6]Glc$, and here the fitting of model parameters to the labeled starch (Fig. 3A) resulted in an optimum for $V_{TPC} = 1.0$. Having determined V_{TPC} by two independent experimental approaches, a value of 1.0 was used for subsequent simulations.

Reversible Reactions of the Pentose Phosphate Pathway—After labeling of *B. napus* embryos with $[U-^{13}C_{12}]sucrose/[U-^{13}C_6]Glc$, the fractional labeling of Glc isolated from starch was used to fit the reversible fluxes through TK and TA with the parameters V_{TK} (Fig. 3B) and V_{TA} (Fig. 4A), respectively. To determine whether the labeling experiments were capable of yielding information on possible differences between reversibility constants for the two different reactions of transketolase (as indicated in Table I), experimental data were simulated in two ways. In the first analysis, the two TK reactions had one value of TK for both reactions (V_{TK}); in the second set of simulations, the reversible fluxes of the two TK reactions had two independent values (V_{TK1} and V_{TK2}). There was no significant difference in the goodness of fit between the two analyses, and in the second analysis there was no clear optimum combination of V_{TK2} and TK2. Therefore, one parameter, V_{TK} , was used for both TK reactions for all subsequent simulations.

Fig. 4A shows the best fit value for V_{TK} and V_{TA} , with $X = 0.12$. If X decreases, V_{TK} and V_{TA} change (Fig. 4A). The best fit value of V_{TA} is rather sensitive to the exact value of X , whereas the value of V_{TK} is not. The independent determination of X by labeling with $[1,2-^{13}C_2]Glc$ (see below) allows a global optimum for X , V_{TPC} , V_{TK} , and V_{TA} to be found, since optimal fit for the labeling in Glc, labeled from $[U-^{13}C_{12}]sucrose/[U-^{13}C_6]Glc$ and for the ratio m_1/m_2 in C18:1₍₁₋₂₎ (labeling with $[1,2-^{13}C_2]Glc$) cross (Fig. 4B).

As shown in Fig. 6, using the above optimal values, the model calculates mass distributions that agree very well with the fractional labeling measured in Glc (from starch), glycerol, and histidine, representing Glc-6-P, cytosolic DHAP, and pentose phosphate, respectively. The fact that parameters obtained by fitting the labeling in one set of metabolites yield simulations that agree well with labeling in different metabolites supports the validity of the model and the metabolic network (Fig. 2). Since histidine includes the carbon chain of pentose phosphate plus one carbon from C-1 metabolism, the difference in m_1 can be explained by the labeling in this extra carbon (Fig. 6).

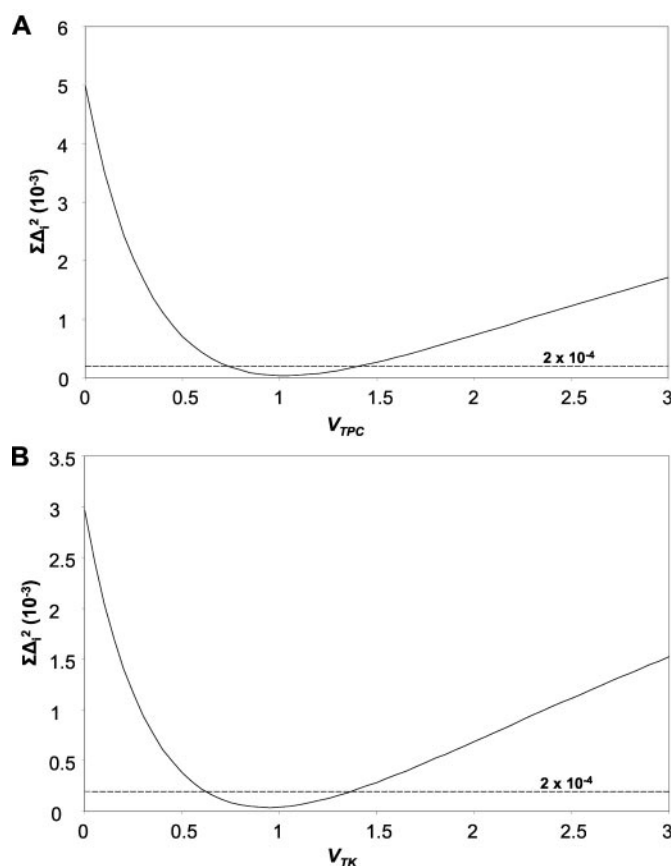


FIG. 3. Least square fitting of the model parameters V_{TK} (A) and V_{TPC} (B) to experimental data. Embryos were labeled for 14 days with $[U-^{13}C_{12}]$ sucrose/ $[U-^{13}C_6]$ Glc (see “Experimental Procedures”). Labeling in the glucosyl units of starch was measured by GC/MS (see “Experimental Procedures”). The measured fractional enrichment in fragments $Glc_{(1-2)}$, $Glc_{(3-6)}$, and $Glc_{(1-6)}$ was compared with fractional enrichments predicted by the model. A, the sum of squared differences ($\Sigma\Delta_i^2$; see “Experimental Procedures”) was calculated for a range of values for V_{TPC} while keeping the other parameters constant ($X = 0.12$, $V_{TA} = 0.01$, $V_{TK} = 0.95$). B, the sum of squared differences was calculated for a range of values of V_{TK} ($X = 0.12$, $V_{TA} = 0.01$, $V_{TPC} = 1$). The 2×10^{-4} level for the sum of squared S.D. values of the GC/MS measurements for all isotopomers. This threshold was used to estimate confidence intervals for the values (Table IV). V_{TPC} was also determined independently to be between 0.6 and 1.4 by measuring redistribution of label between C-1 and C-6 of hexose phosphate (Table II).

Because the flux through the OPPP is low ($X = 0.12$; see below), the value for the reversible flux V_{TK} (0.95) is almost 10 times higher than the net flux through TK (which is equal to X ; Table I). The reversible flux, V_{TPC} (1.0), is similar to the net flux through glycolysis ($1 - X = 0.88$). For the reversible TA flux, the value $V_{TA} = 0.01$ was obtained, which is negligible compared with the net forward flux through OPPP (Table I). Since V_{TK} and V_{TPC} are large reversible fluxes, the impact of TK and triose/hexose cycling on the labeling pattern shown in Fig. 6 can be qualitatively explained. TK reversibly exchanges two-carbon units between Fru-6-P, Xu-5-P, and other ketose phosphates, so that the abundance of $[1,2-^{13}C_2]$ Fru-6-P increases at the expense of $[U-^{13}C_6]$ Fru-6-P, contributing to the abundances of m_2 isotopomers in $Glc_{(1-6)}$ (Fig. 6). Using the computer simulation, the same effect can be seen for m_2 of the triose phosphate and pentose phosphate derivatives. By contrast, the abundance of m_3 isotopomers (Fig. 6) of $Glc_{(1-6)}$ is largely attributed to triose/hexose cycling. Thus, the labeling patterns of all of the metabolites shown in Fig. 6 reveal the signature of reversible TK and of triose/hexose cycling.

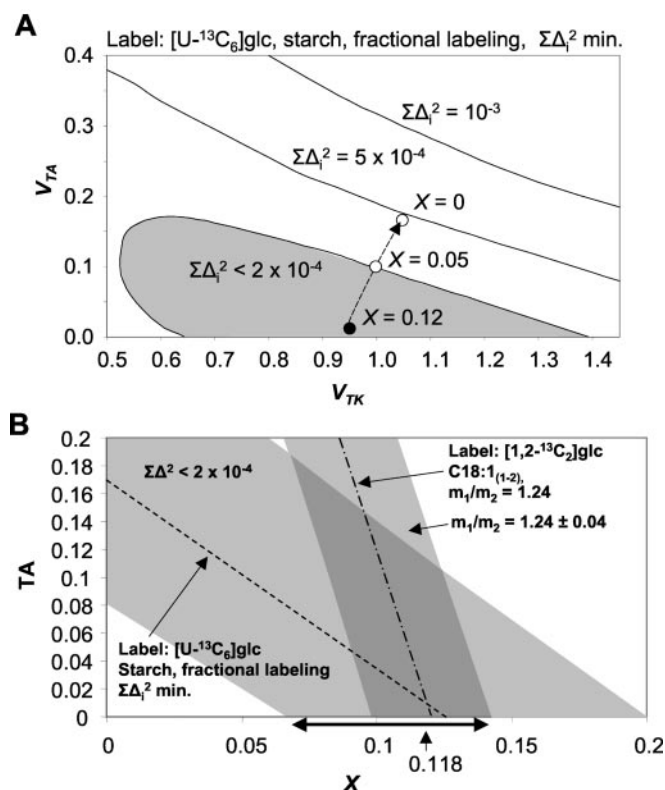


FIG. 4. Optimized flux parameter values and obtaining a global solution by experimental over determination. Embryos were labeled for 14 days with $[U-^{13}C_{12}]$ sucrose/ $[U-^{13}C_6]$ Glc. Glc obtained by starch hydrolysis was derivatized and analyzed by GC/MS (see “Experimental Procedures”). The measured fractional enrichment in fragments $Glc_{(1-2)}$, $Glc_{(3-6)}$, and $Glc_{(1-6)}$ was compared with the fractional enrichments predicted by the model. The sum of squared differences ($\Sigma\Delta_i^2$; see “Experimental Procedures”) was calculated for a range of values in the V_{TK}/V_{TA} plane, with $V_{TPC} = 1.0$. A, contour map showing lines of equal $\Sigma\Delta_i^2$ in the V_{TK}/V_{TA} plane. These contour lines were calculated using $V_{TPC} = 1$ and $X = 0.12$. The contour line of $\Sigma\Delta_i^2 = 2 \times 10^{-4}$ surrounds an area (shaded) that corresponds to the limits of confidence that we place around the combination of V_{TK} and V_{TA} values (black point), which gives the best fit to the experimental data (where $\Sigma\Delta_i^2$ has its minimum). Depending on the value of X , the best fit combination of V_{TK} and V_{TA} changes (dashed arrow). Two such additional points are shown that correspond to V_{TK}/V_{TA} values that yield minima in $\Sigma\Delta_i^2$ when $X = 0.05$ and $X = 0$ (open circles). B shows the results of optimization of the fit for V_{TA} and X for the same experiment and for A. In this case, there is no single minimum for $\Sigma\Delta_i^2$ but instead a set of points indicated by the dashed line with a confidence area again based on a 2×10^{-4} threshold for $\Sigma\Delta_i^2$ shaded in gray. The results of optimizing the fit for V_{TA} and X for an experiment with $[1,2-^{13}C_2]$ Glc/ $[1-^{13}C]$ Glc (1:1) are also shown in B. In this case, mass spectroscopic data from C18:1(1-2) showing a m_1/m_2 ratio of 1.24 ± 0.04 ($n = 3$ independent experiments) was measured. A second dashed line shows the set of V_{TA}/X points for which the simulated m_1/m_2 ratio matches the experimental value best. The area where $m_1/m_2 = 1.24 \pm 0.04$ is indicated in gray. The two sets of optimized values for X and V_{TA} for the two experiments intersect at $X = 0.12$, $V_{TA} = 0.01$. This point defines a single overall optimum for the parameters X , V_{TK} , V_{TA} , and V_{TPC} . The resulting confidence interval for X is indicated by a double-headed arrow along the x axis.

Equilibration of Pentose Phosphate Pools—Histidine is derived from Rib-5-P, which can be synthesized by two metabolic routes. The first route is the oxidative decarboxylation of Glc-6-P; in the second route, TK forms Xu-5-P, from which ribulose-5-phosphate-3-epimerase makes Ru-5-P, and this in turn is acted upon by ribose-5-phosphate isomerase to form Rib-5-P. After labeling with $[U-^{13}C_{12}]$ sucrose/ $[U-^{13}C_6]$ Glc, flux through the first route produces the m_5 isotopomer of His $_{(1-6)}$, and flux through the TK route produces m_2 and m_3 isotopomers. Since the m_5 isotopomer is only about one-quarter as abundant as the

TABLE IV
Relationship between the metabolic fluxes and the observations from which they are calculated

The flux parameters as described in Fig. 2 and Table I were determined by using different labeled substrates and by analyzing different metabolites. Confidence intervals are estimated as described in Figs. 3 and 4.

Flux parameter	Labeled substrate supplied	Most informative metabolites	Value (confidence interval)
X	[1,2- ¹³ C ₂]Glc	Starch, glycerol, Ala, Val, C18:1	0.12 (0.07–0.14)
V_{TK}	[U- ¹³ C ₆]Glc	Starch	0.95 (0.5–1.4)
V_{TA}	[U- ¹³ C ₆]Glc	Starch	0.01 (0–0.17)
V_{TPC}	[1- ¹³ C]Glc, [6- ¹³ C]Glc	Suc, starch	0.6–1.4
V_{TPC}	[U- ¹³ C ₆]Glc	Starch	1.0 (0.7–1.4)

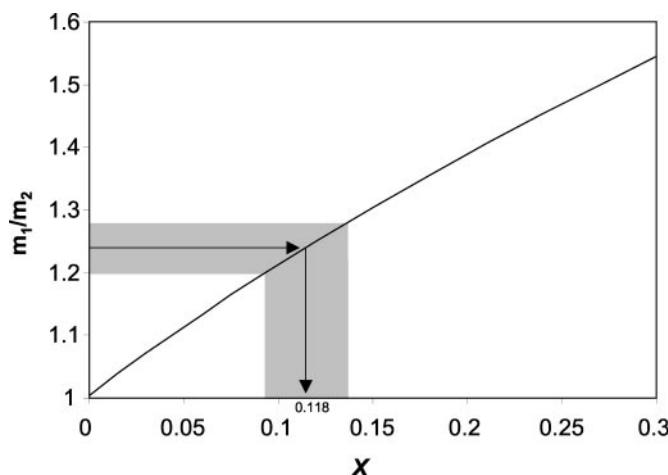


FIG. 5. Relation between the m_1/m_2 ratio in C18:1₍₁₋₂₎ and X , after labeling with [1-¹³C]Glc/[1,2-¹³C₂]Glc (1:1). After labeling with [1-¹³C]Glc/[1,2-¹³C₂]Glc (1:1), the ratio m_1/m_2 in C18:1₍₁₋₂₎ was determined by GC/MS. The ratio m_1/m_2 was simulated dependent on X , with the parameters $V_{TK} = 0.95$, $V_{TPC} = 1.0$, and $V_{TA} = 0.01$. The horizontal line with the gray bar denotes the measured value with the S.D. (1.24 ± 0.04 , $n = 3$ independent experiments), and the vertical gray bar denotes the uncertainty in the derived value of X that corresponds to this experimental range.

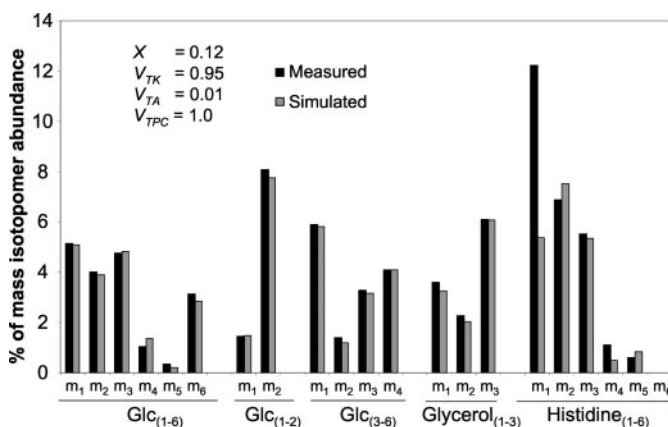


FIG. 6. Comparison of measured and simulated MS data. Embryos were grown for 14 days with [U-¹³C₁₂]sucrose/[U-¹³C₆]Glc (see “Experimental Procedures”). Labeling in glucosyl units of starch, in glycerol from TAG, and in amino acids from seed protein was analyzed by GC/MS (see “Experimental Procedures”). The measured isotopomer abundances for the fragments Glc₍₁₋₂₎, Glc₍₁₋₆₎, Glc₍₃₋₆₎, glycerol₍₁₋₃₎, and His₍₁₋₆₎ are shown as black bars. With the flux parameters $X = 0.1$, $V_{TPC} = 1.0$, $V_{TK} = 0.95$, and $V_{TA} = 0.01$ (see Fig. 4), the model yields simulated fractional labeling for hexose phosphate, triose phosphate, and pentose phosphate (gray bars). Good agreement between experimental and simulated isotopomer levels is seen except for histidine m_1 . Since histidine comprises the carbon chain of pentose phosphate plus one carbon from C-1 metabolism, the difference in m_1 can be explained by the labeling in this extra carbon.

m_6 isotopomer in Glc₍₁₋₆₎ (Fig. 6) and is much less abundant than the m_2 and m_3 isotopomers, most of the histidine must be synthesized via the TK route. Since the TK signature is produced

first in Xu-5-P molecules, the flux from Xu-5-P \rightarrow Ru-5-P \rightarrow Rib-5-P must be much larger than the flux from Glc-6-P \rightarrow Ru-5-P \rightarrow Rib-5-P. This implies that the reversible ribulose-5-phosphate-3-epimerase and ribose-5-phosphate isomerase fluxes are substantially higher than the flux through oxidative decarboxylation, which has a magnitude of $3X$ in the notation of our model. This supports the model assumption (Fig. 2) that the pentose phosphates are in isotopic equilibrium and may be treated as one pool.

Quantification of the Split of Carbon Flux between Glycolysis and OPPP (X)—The results of labeling with [1,2-¹³C₂]Glc are particularly sensitive to the OPPP flux (Fig. 5), and this substrate was therefore used (Table III) in addition to the experiments described above using uniformly ¹³C-labeled sugars. When metabolized by glycolysis, double-labeled [1,2-¹³C₂]Glc produces the double-labeled intermediates [2,3-¹³C₂]triose phosphate, [2,3-¹³C₂]pyruvate, and [1,2-¹³C₂]acetyl-CoA, resulting in m_2 mass peaks (e.g. in the fragment C18:1₍₁₋₂₎). However, oxidative decarboxylation of [1,2-¹³C₂]Glc-6-P produces [1-¹³C]pentose phosphate, which is then converted via TK and TA reactions to singly labeled fructose ([1-¹³C]Fru-6-P, [3-¹³C]Fru-6-P) and subsequently to other singly labeled intermediates that contribute to m_1 abundance in mass spectra. The more [1,2-¹³C₂]Glc is converted to single labeled hexose phosphate by the OPPP, the higher the ratio m_1/m_2 (¹³C₁/¹³C₂) in triose phosphate derivatives and in acetate units of fatty acids (Fig. 5). The ratio m_1/m_2 was measured by mass spectrometry. In addition to labeling with [1,2-¹³C₂]Glc alone, mixtures of [1,2-¹³C₂]Glc with [1-¹³C]Glc or [6-¹³C]Glc were used. The action of glycolysis on a 1:1 mixture of [1,2-¹³C₂]Glc and [1-¹³C]Glc will produce an m_1/m_2 ratio of 1, whereas OPPP flux will result in an m_1/m_2 ratio of >1 (Fig. 5), which was indeed observed (Table III). The results of using a mixture of [1,2-¹³C₂]Glc and [6-¹³C]Glc (1:1) would be sensitive to any disequilibrium at triose phosphate isomerase and provide information on triose/hexose cycling. For this experiment, a m_1/m_2 ratio lower than 1 was found for Glc₍₁₋₂₎ (Table III), which is to be expected, because only about 20% of the label in C-6 of hexose phosphate is redistributed to C-1 of hexose phosphate by triose cycling (Table II).

After labeling with [1,2-¹³C₂]Glc/[1-¹³C]Glc (1:1), the fragment C18:1₍₁₋₂₎ was measured by GC/MS, and an average value for m_1/m_2 of 1.24 ± 0.04 was found ($n = 3$). As described in the legend to Fig. 4B, this value corresponds to $X = 0.12$ (0.07–0.14). The m_1/m_2 ratios were also measured for several metabolites derived from intermediates of the pathway of Glc breakdown (Table III) after labeling with [1,2-¹³C₂]Glc or with [1,2-¹³C₂]Glc/[6-¹³C]Glc (1:1). Again, the computer simulation predicted m_1/m_2 ratios for different intermediates of the different substrate labeling experiments that were similar to the measured values (Table III).

DISCUSSION

The construction of a metabolic network (Fig. 1) for developing *B. napus* embryos was possible because extensive literature allowed the assumptions of pathways and subcellular localiza-

tion to be justified. On this basis, a flux model for glycolysis/OPPP was constructed, which was used to interpret the results of labeling experiments (Fig. 2) and to determine relative flux of carbon through a number of key reactions and intermediates. The flux model was implemented as a computer program that simulates labeling patterns in intermediates based on given flux parameters. Glc labeled in different positions was used for the steady state labeling experiments (Table IV). Most of the combined metabolic pools and the connections between them incorporated in the flux model could be verified based on the results of the labeling experiments. Flux parameters for reversibility of TK (V_{TK}), TA (V_{TA}), and the cleavage of hexose phosphate into, and resynthesis from, triose phosphate (V_{TPC}) were determined by optimizing the agreement between model-generated output data and labeling patterns measured in different biosynthetic products (Figs. 3–5). The proportion of the Glc taken up that was metabolized through OPPP versus glycolysis (model parameter X) was then determined as a measure of net flux through OPPP.

The interdependence of the values obtained for X and V_{TA} , as shown in Fig. 4, emphasizes that in the metabolic network glycolysis/OPPP, the contribution of the OPPP cannot be determined without taking account of the reversibilities of the nonoxidative reactions. The problem becomes that of finding a global optimum in a four-dimensional parameter space (X , V_{TK} , V_{TA} , V_{TPC}). This was achieved by overdetermination of the flux model both by analysis of multiple metabolic products and by labeling embryos in different experiments with Glc labeled in different positions.

Several previous studies have attempted to address the contributions of OPPP to metabolism in plant and other cells. Early methods based on differential release of $^{14}\text{CO}_2$ from $[1-^{14}\text{C}]\text{Glc}$ and $[6-^{14}\text{C}]\text{Glc}$ suffer from limitations due to (a) refixation of CO_2 , (b) failure to account for the effects of TK and TA reversibility, (c) the effects of cyclic flux, and (d) the contributions of mitochondrial respiration to CO_2 release. For example, $^{14}\text{CO}_2$ release from ^{14}C Glc by castor bean endosperm (73) suggested that 50–70% of NADPH needed for fatty acid synthesis can be provided by OPPP. However, that study applied a simplified flux model without consideration of resynthesis of Fru-6-P from triose phosphate. Without modeling the OPPP/glycolysis network, the determination of OPPP flux is prone to major errors (30). Other studies based on the distribution of activity from $[1-^{14}\text{C}]\text{Glc-6-P}$ into starch, CO_2 , and fatty acids by isolated plastids also suggested substantial OPPP activity of developing *B. napus* embryos (3). However, since there is evidence that the major carbon influx into the plastid *in vivo* occurs at the level of PEP or pyruvate or triose phosphate (3, 9, 14, 46), the fate of label supplied to isolated plastids as Glc-6-P will not accurately reflect the OPPP flux *in vivo*.

The use of $[1,2-^{13}\text{C}_2]\text{Glc}$ *in vivo*, alone and in combination with other ^{13}C substrates, and the use of computer modeling addresses the above limitations. In particular, the impact of TA and TK reversibilities can be assessed.

In developing *B. napus* seeds, most of the carbon entering the OPPP/glycolysis network is metabolized to pyruvate, acetyl-CoA, and finally fatty acids. Based on the flux model used in this study (Fig. 2, Table I) one can determine how much of the NADPH needed for fatty acid synthesis is provided by the OPPP. The glycolysis/OPPP split was determined as $X = 0.12$ (0.07–0.14) (Table IV). According to the flux model (Fig. 2, Table I), the efflux of C_3 units into fatty acid synthesis is $2 - X$ (equal to 1.88 (1.86–1.93)), whereas the amount of NADPH produced by glucose-6-phosphate dehydrogenase and phosphogluconate dehydrogenase is $6X$ (equal to 0.72 (0.42–0.84)). Because the elongation of a fatty acid chain by one C_2 unit uses

two reduction equivalents (one NADPH by ketoacyl-ACP reductase and one NADH by enoyl-ACP reductase), there is demand for the rate of production of NADPH to be 1.88 and the same for NADH production. The pyruvate dehydrogenase reaction meets the NADH demand. OPPP produces 0.72/1.88 (38%) of the NADPH required for fatty acid synthesis (confidence range is 22–45%). To produce all the NADPH required, X would have to be 0.286, which is incompatible with the labeling patterns (see, for example, Fig. 5).

Our conclusion of a limited role for OPPP in oilseed NADPH production is perhaps surprising, considering the general conclusions of most previous studies on oilseed metabolism (3, 73). However, other sources of reductant such as glycolysis, light reactions of photosynthesis, and the mitochondrial metabolism may supply this need. Glycolysis, together with the subsequent formation of acetyl-CoA by pyruvate dehydrogenase complex (PDH), produces 2 mol of reductant for each mol of acetyl-CoA (during the steps catalyzed by GAPDH and PDH) and 1 mol of ATP (at GAPDH). Thus, glycolysis could in principle provide all of the carbon and cofactors for fatty acid synthesis without the need for additional production of NADPH. Plastid GAPDH can produce NADPH, or cytosolic NADH could either be converted to NADPH or used directly for fatty acid synthesis. Indeed, there is evidence for different transhydrogenase and transport systems for NAD(P)H across the inner plastid membrane and for NADH utilization in plastidial anabolism (74, 75).

Although glycolysis can meet the demands of fatty acid synthesis for cofactors, the consumption of ATP and NAD(P)H by transport processes or other cell “maintenance” functions or futile cycles must demand additional production of cofactors. In this regard, another potential source of plastid NADPH is photosynthesis. The labeling experiments described here were performed with a low light intensity (continuous light, $50 \mu\text{mol m}^{-2} \text{s}^{-1}$) to simulate the degree of penetration of sunlight through the silique wall and the seed coat. Under these conditions, the embryos are green during growth, as they are *in planta*. Indeed, calculations indicate that this amount of light could substantially contribute to NADPH production via the photosynthetic light reactions (10).

The low value for V_{TA} (Table IV) may also be associated with the photosynthetic potential of *B. napus* embryos (76). One can assume that in chloroplasts TA activity is limited to the minimum needed for OPPP flux, because the TA reaction interferes with the regenerative phase of the photosynthetic reduction cycle and produces a futile cycle. In photosynthesis, recycling of pentose phosphate is in part provided by a reaction sequence comprising aldolase (erythrose-4-phosphate + GAP → sedoheptulose-1,7-bisphosphate), sedoheptulose bisphosphatase, and TK (sedoheptulose 7-phosphate + GAP → Rib-5-P + Xu-5-P). By adding TA to this reaction network, sedoheptulose 7-phosphate can be cyclically removed (sedoheptulose 7-phosphate + GAP → erythrose 4-phosphate + Fru-6-P) and regenerated from sedoheptulose 1,7-bisphosphate, resulting in a futile cycle that hydrolyzes sugar-phosphates. The assumption of relatively low TA activity in chloroplasts is supported by Thom *et al.* (77), who report a major increase of TA activity during the transition from chloroplasts to chromoplasts in ripening red pepper fruits. Inhibition of TA activity in chloroplasts could be mediated via light (78). The action of the full Calvin cycle is not consistent with the labeling patterns we observed, but ribulose-1,5-bisphosphate carboxylase/oxygenase activity is present in *B. napus* embryos (10), which could produce a flux between Ru-5-P and 3-phosphoglyceric acid. However, none of the parameters derived in this study would be affected by such a flux. In order to test this possibility, labeling and other experiments are under way, which have the sensitivity to detect ribulose-

TABLE V
Steady state equations for the isotopomers of metabolic pools

The isotopomer vectors of hexose 6-phosphate, pentose 6-phosphate, sedoheptulose 7-phosphate, erythrose 4-phosphate, and triose phosphate are named HP_i , PP_i , SP_i , EP_i , and TP_i , respectively, where the index i defines a particular isotopomer, with $i = 0 \dots n$; $n = 63, 31, 127, 15$, and 7 for HP_i , PP_i , SP_i , EP_i , and TP_i , respectively (for a molecule with n carbon atoms, there are 2^n possible combinations of ^{12}C and ^{13}C atoms). The equation system uses the flux parameters X , V_{TK} , V_{TA} , V_{TPC} , and the isotopomer abundances derived from the biochemical reactions outlined in Table I (e.g. HP_TA_i = abundance of hexose-phosphate isotopomer i from transaldolase reaction). Glc_in , input of labeled Glc; HP_TK2 , hexose phosphate from transketolase 2, respectively; HP_TA , hexose phosphate from TA. $PP_TK1back_i$, pentose phosphate from transketolase 1, back-reaction; $PP_TK2back_i$, pentose phosphate from transketolase 2, back-reaction; PP_decarb_i , pentose phosphate from HP by oxidative decarboxylation. EP_TA_i , erythrose 4-phosphate from transaldolase; $EP_TK2back_i$, erythrose-4-phosphate from transketolase 2, back-reaction; EP_TK2_i , erythrose 4-phosphate from transketolase 2, back-reaction. SP_TK1_i , sedoheptulose-7-P from transketolase 1; SP_TAback_i , sedoheptulose 7-phosphate from transaldolase, back-reaction. TP_kin_i , triose-P from hexose-P by aldolase; TP_TK2_i , triose phosphate from transketolase 2; TP_TK1_i , triose phosphate from transketolase 1; TP_TAback_i , triose-P from transaldolase, back-reaction.

Influx	Efflux
$\Delta HP_i = Glc_in_i + HP_TK2_i^*(X + V_{\text{TK}}) + HP_TA_i^*(X + V_{\text{TA}}) + HP_Aldo_i^*V_{\text{TPC}}$	$-HP_i^*(1 + 2X + V_{\text{TK}} + V_{\text{TA}} + V_{\text{TPC}})$
$\Delta PP_i = PP_TK1back_i^*2V_{\text{TK}} + PP_TK2back_i^*V_{\text{TK}} + PP_decarb_i^*3X$	$-PP_i^*(3X + 3V_{\text{TK}})$
$\Delta EP_i = EP_TA_i^*(X + V_{\text{TA}}) + EP_TK2back_i^*V_{\text{TK}}$	$-EP_i^*(2X + V_{\text{TA}} + V_{\text{TK}})$
$\Delta SP_i = SP_TK1_i^*(X + V_{\text{TK}}) + SP_TAback_i^*V_{\text{TA}}$	$-SP_i^*(X + V_{\text{TK}} + V_{\text{TA}})$
$\Delta TP_i = TP_kin_i^*(2*(1 - X + V_{\text{TPC}})) + TP_TK2_i^*(X + V_{\text{TK}}) + TP_TK1_i^*(X + V_{\text{TK}}) + TP_TAback_i^*V_{\text{TA}}$	$-TP_i^*(2V_{\text{TK}} + V_{\text{TA}} + 2 + 2V_{\text{TPC}})$

1,5-bisphosphate carboxylase/oxygenase-specific isotopomer patterns and *in vivo* activation status.

Potential Limitations of This Study—By closely mimicking *in vivo* growth conditions, we have aimed to obtain information on metabolic fluxes relevant to the developing embryo in a plant. The culture conditions are such that an embryonic mode of growth is preserved, and the embryos kept in culture achieve similar oil and protein content as well as similar fatty acid composition to *in planta* seeds (22). In addition, the embryos from culture are viable and able to germinate if transferred to a different culture medium. Under the low light conditions used in the labeling experiments, the embryos remain green during culture, which indicates that they maintain their principally chloroplast-like plastid structure. Nevertheless, growth in culture and any flux model of metabolism must represent an approximation of true *in vivo* conditions. We present some of the possible limitations to the model presented in this study and efforts to address them.

First, the assumptions of isotopic steady state and metabolic homogeneity are at the heart of flux analyses based on steady state labeling patterns, and they are far more difficult to achieve in plant tissues than in microorganisms. In this study, developing *B. napus* embryos were dissected from siliques at 20 days after flowering and cultured during the main phase of oil accumulation under conditions close to *in planta* growth. Since it is reported that the Suc/hexose ratio changes in the liquid endosperm surrounding the developing embryos during development (22, 23), metabolic steady state may not be achieved for sucrose and Glc metabolism. However, the embryos in our experiments are initiated into culture when a high sucrose/Glc ratio already exists and are maintained at a constant ratio (22).

This model system for embryo metabolism has several characteristics that allow a close approximation to metabolic and isotopic steady state. Cell divisions are essentially complete by the start of the labeling period, and therefore embryo growth consists almost entirely of cell expansion with production of storage products. Although there are different cell types in a growing embryo, the tissue is dominated by the cotyledon cells, which produce the storage reserves. In these cells, the major metabolic fluxes are directed toward the production of oil and storage proteins, which represent stable end products. Therefore, turnover of polymers is not a major complicating flux, and overall metabolism may be less complex than in rapidly dividing cells of, for example, root tips or cell suspensions. Evidence for steady state conditions was provided by comparison of labeling patterns and levels after 3 and 14 days, which indicated that isotopic steady state was achieved within 3 days for inter-

mediate pools (sucrose, free amino acids) and also for starch. Furthermore, although the embryos when placed in culture already have some storage TAG and protein that is not turned over, after the full 14-day labeling period, TAG and protein increased over 10-fold, resulting in essentially complete labeling of accumulated end products. No evidence of multiple pools in any of the storage products (starch, protein, oil, sucrose) was observed, which again probably reflects the fact that the embryo is dominated by cotyledon cells and that exposure to constant labeling conditions in the external medium allowed the principal metabolic fluxes to be investigated.

Second, for developing seeds of *B. napus*, oil accumulation overlaps with but slightly precedes storage protein accumulation. Thus, the isotopomer imprint accumulated in seed protein could in part reflect metabolism after the peak phase of oil synthesis. However, the 14-day culture of our experiments covers the main period of oil accumulation and not the later phase that is more dominated by storage protein formation (22). Thus, the isotopic imprint in protein represents metabolism during the phase of maximal oil synthesis. Accordingly, we observed that the acetate units in fatty acids (from seed oil) and homologue C_2 units in amino acids (from storage protein) were almost identically labeled (see Table III).

Finally, the OPPP can operate in a cyclic manner in root plastids, probably without net contribution of the upper part of hexose phosphate molecules to further metabolism (79). This could distort the derived value of X if [$1\text{-}^{13}\text{C}$]pentose phosphate, produced by oxidative decarboxylation of [$1,2\text{-}^{13}\text{C}_2$]Glc-6-P, is recycled to produce single ^{13}C -labeled Fru-6-P that does not enter the glycolytic route leading to fatty acids and therefore would not contribute to the measured isotopomer pattern in glycolytic products. This kind of “sequestered” cyclic OPPP is not supported by the labeling pattern of histidine, which is derived from plastidic pentose phosphate or by the similar m_1/m_2 ratios between $\text{Glc}_{(1-2)}$, $\text{Ala}_{(2-3)}$, and $\text{C18:1}_{(1-2)}$ (Table III).

Conclusions—Plant seeds provide the major food and economic value of most crops, and therefore a quantitative understanding of their metabolic networks is an important goal for plant biochemists. Using steady-state stable isotope labeling, we have developed and tested a model describing flux through *B. napus* embryo glycolysis and OPPP. Computer simulation allowed the complex interaction of reversible fluxes to be fit to experimental data. The reliability of the determination of OPPP and other fluxes in this study was enhanced by using a well studied system that allows the achievement of steady state labeling, through the use of multiple substrates, with the analysis of multiple products, and by the testing of underlying assumptions inherent in such models. Although future im-

improvements can be anticipated, we believe this to be the most reliable analysis to date of the OPPP/glycolysis network in a plant system.

Acknowledgments—We are indebted to Dr. Mike Pollard and Dr. Sari Ruuska (Michigan State University) for helpful discussions.

APPENDIX

A computer program was used to simulate the steady state distribution of isotopomers in the intermediate metabolite pools of the flux model (Fig. 2) using a linear equation system that employs the dimensionless flux parameters (Table V). The isotopomers of the intermediate pools are represented as “isotopomer distribution vectors” as described by Schmidt *et al.* (66). For each biochemical reaction (Table I), the rate of synthesis of each possible isotopomer of the products of that reaction is calculated by multiplication of the vectors representing a subset of the isotopomers of the reactants by “isotopomer mapping matrices” (66). For each product isotopomer, the reactant isotopomers are combined according to probabilistic relations. The carbon transitions that underlie the different reactions can be found in standard biochemistry textbooks.

An iterative calculation process is used by the program, starting with all intermediate pools unlabeled and proceeding to calculate the effects of the influx of labeled Glc into the system. Each cycle of the iterative process consists of 3 steps: (a) calculation of the contributions to the isotopomer abundances from each biochemical reaction, based on the current state of the intermediate pools (*e.g.* HP_TA represents hexose phosphate from TA); (b) calculation of the net change in the abundance of each isotopomer (*e.g.* ΔHP_i represents sum of influx and efflux into isotopomer HP_i ; see Table V); and (c) calculation of new isotopomer values for the intermediate pools (*e.g.* $\text{HP}_i = \text{HP}_i + f^* \Delta\text{HP}_i$; typically $f = 0.001$). The iterative process typically requires 2000–5000 iterative cycles to reach steady state, which is defined as being achieved when the sum of all influxes and effluxes into all 248 isotopomers is below an arbitrary threshold (typically 10^{-12}).

REFERENCES

- Hill, L. M., and Rawsthorne, S. (2000) *Biochem. Soc. Trans.* **28**, 667–669
- Kubis, S. E., and Rawsthorne, S. (2000) *Biochem. Soc. Trans.* **28**, 665–666
- Eastmond, P. J., and Rawsthorne, S. (2000) *Plant Physiol.* **122**, 767–774
- Eastmond, P. J., and Rawsthorne, S. (1998) *J. Exp. Bot.* **49**, 1105–1111
- Dasilva, P. M. F. R., Eastmond, P. J., Hill, L. M., Smith, A. M., and Rawsthorne, S. (1997) *Planta* **203**, 480–487
- Eastmond, P. J., Dennis, D. T., and Rawsthorne, S. (1997) *Plant Physiol.* **114**, 851–856
- Eastmond, P., Kolaena, L., and Rawsthorne, S. (1996) *J. Exp. Bot.* **47**, 1763–1769
- Kang, F., and Rawsthorne, S. (1996) *Planta* **199**, 321–327
- Kang, F., and Rawsthorne, S. (1994) *Plant J.* **6**, 795–805
- King, S. P., Badger, M. R., and Furbank, R. T. (1998) *Austr. J. Plant Physiol.* **25**, 377–386
- King, S. P., Lunn, J. E., Badger, M. R., and Furbank, R. T. (1997) *Plant Physiol.* **114**, 318
- King, S. P., Lunn, J. E., and Furbank, R. T. (1997) *Plant Physiol.* **114**, 153–160
- Singh, D. K., Malhotra, S. P., and Singh, R. (2000) *Indian J. Biochem. Biophys.* **37**, 51–58
- Gupta, R., and Singh, R. (1997) *Indian J. Biochem. Biophys.* **34**, 288–295
- Gupta, R., and Singh, R. (1996) *J. Biosci.* **21**, 819–826
- Gupta, R., and Singh, R. (1996) *J. Plant Biochem. Biotechnol.* **5**, 127–130
- Talwar, G., Dua, A., and Singh, R. (1996) *Photosynthetica* **32**, 221–229
- Mehta, M., Saharan, M. R., and Singh, R. (1995) *J. Plant Biochem. Biotechnol.* **4**, 11–16
- Singal, H. R., Talwar, G., Dua, A., and Singh, R. (1995) *J. Biosci.* **20**, 49–58
- Singal, H. R., Sheoran, I. S., and Singh, R. (1987) *Plant Physiol.* **83**, 1043–1047
- Bao, X., Pollard, M., and Ohlrogge, J. B. (1998) *Plant Physiol.* **118**, 183–190
- Schwender, J., and Ohlrogge, J. (2002) *Plant Physiol.* **130**, 347–361
- Hill, L. M., Morley-Smith, E. R., and Rawsthorne, S. (2003) *Plant Physiol.* **131**, 24
- Thelen, J. J., and Ohlrogge, J. B. (2002) *Metab. Eng.* **4**, 12–21
- Katz, J., Landau, B. R., and Bartsch, G. E. (1966) *J. Biol. Chem.* **241**, 727–740
- Geer, B. W., Lindel, D. L., and Lindel, D. M. (1979) *Biochem. Genet.* **17**, 881–895
- Sheldon, P. S., Kekwick, R. G. O., Smith, C. G., Sidebottom, C., and Slabas, A. R. (1992) *Biochim. Biophys. Acta* **1120**, 151–159
- Slabas, A. R., Sidebottom, C. M., Hellyer, A., Kessel, R. M. J., and Tombs, M. P. (1986) *Biochim. Biophys. Acta* **877**, 271–280
- Neuhaus, H. E., and Emes, M. J. (2000) *Annu. Rev. Plant Physiol. Plant Mol. Biol.* **51**, 111–140
- Roscher, A., Kruger, N. J., and Ratcliffe, R. G. (2000) *J. Biotechnol.* **77**, 81–102
- Dieuaide-Noubhani, M., Raffard, G., Canioni, P., Pradet, A., and Raymond, P. (1995) *J. Biol. Chem.* **270**, 13147–13159
- Edwards, S., Nguyen, B. T., Do, B., and Roberts, J. K. M. (1998) *Plant Physiol.* **116**, 1073–1081
- Fernie, A. R., Roscher, A., Ratcliffe, R. G., and Kruger, N. J. (2001) *Planta* **212**, 250–263
- Rontein, D., Dieuaide-Noubhani, M., Dufourc, E. J., Raymond, P., and Rolin, D. (2002) *J. Biol. Chem.* **277**, 43948–43960
- Szyperski, T. (1998) *Q. Rev. Biophys.* **31**, 41–106
- Dauner, M., and Sauer, U. (2000) *Biotechnol. Prog.* **16**, 642–649
- Wittmann, C., and Heinzle, E. (1999) *Biotechnol. Bioeng.* **62**, 739–750
- Fernie, A. R., Roessner, U., and Geigenberger, P. (2001) *Plant Physiol.* **125**, 1967–1977
- Folch, J., Lees, M., and Sloane-Stanley, G. H. S. (1951) *J. Biol. Chem.* **226**, 497–509
- Bao, X. M., Focke, M., Pollard, M., and Ohlrogge, J. (2000) *Plant J.* **22**, 39–50
- Browse, J., McCourt, P., and Somerville, C. (1986) *Anal. Biochem.* **152**, 141–145
- Das Neves, H. J. C., and Vasconcelos, A. M. P. (1987) *J. Chromatogr.* **392**, 249–258
- Lee, W. N. P., Byerley, L. O., Bergner, E. A., and Edmond, J. (1991) *Biol. Mass Spectrom.* **20**, 451–458
- Neese, R. A., Benowitz, N. L., Hoh, R., Faix, D., LaBua, A., Pun, K., and Hellerstein M. K. (1994) *Am. J. Physiol.* **267**, E1023–E1034
- Shachar-Hill Y., and Pfeffer P. E. (1996) *Nuclear Magnetic Resonance in Plant Biology*, pp. 196–250, American Society of Plant Physiologists, Rockville, MD
- Ruuska, S., Girke, T., Benning, C., and Ohlrogge, J. B. (2002) *Plant Cell* **14**, 1191–1206
- Beckles, D. M., Smith, A. M., and Ap Rees, T. (2001) *Plant Physiol.* **125**, 818–827
- Eicks, M., Maurino, V., Knappe, S., Flugge, U. I., and Fischer, K. (2002) *Plant Physiol.* **128**, 512–522
- Schnarrenberger, C., Flechner, A., and Martin, W. (1995) *Plant Physiol.* **108**, 609–614
- Debnam, P. M., and Emes, M. J. (1999) *J. Exp. Bot.* **50**, 1653–1661
- White, J. A., Todd, J., Newman, T., Focks, N., Girke, T., de Ilarduya, O. M., Jaworski, J. G., Ohlrogge, J. B., and Benning, C. (2000) *Plant Physiol.* **124**, 1582–1594
- Ohlrogge, J. B., Kuhn, D. N., and Stumpf, P. K. (1979) *Proc. Natl. Acad. Sci. U. S. A.* **76**, 1194–1198
- Dennis D. T. (1989) in *Physiology, Biochemistry, and Genetics of Nongreen Plastids* (Boyer, C. D., Shannon, R. C., and Hardison, R. C., eds) pp. 120–129, American Society of Plant Physiologists, Rockville, MD
- Domergue, F., Cassagne, C., and Lessire, R. (1999) *Ocl-Ol. Corps Gras Lipides* **6**, 101–106
- Whitfield, H. V., Murphy, D. J., and Hills, M. J. (1993) *Phytochemistry* **32**, 255–258
- Ke, J., Behal, R. H., Back, S. L., Nikolau, B. J., Wurtele, E. S., and Oliver, D. J. (2000) *Plant Physiol.* **123**, 497–508
- Sangwan, R. S., Gauthier, D. A., Turpin, D. H., Pomeroy, M. K., and Plaxton, W. C. (1992) *Planta* **187**, 198–202
- Ohta, D., Fujimori, K., Mizutani, M., Nakayama, Y., Kunpaisal-Hashimoto, R., Münzer, S., and Kozaki, A. (2000) *Plant Physiol.* **122**, 907–914
- Singh B. K. (1999) in *Plant Amino Acids: Biochemistry and Biotechnology* (Singh, B. K., ed) pp. 227–247, Marcel Dekker, New York
- Ho, C. L., Noij, M., and Saito, K. (1999) *J. Biol. Chem.* **274**, 11007–11012
- Schultz C. J., and Coruzzi, G. M. (1995) *Plant J.* **7**, 61–75
- Wilkie, S. E., and Warren, M. J. (1998) *Protein Expression Purif.* **12**, 381–389
- Liepmann, A. H., and Olsen, L. J. (2003) *Plant Physiol.* **131**, 215–227
- Ireland R. J., and Lea J. P. (1999) in *Plant Amino Acids: Biochemistry and Biotechnology* (Singh, B. K., ed) pp. 49–109, Marcel Dekker, New York
- Follstad, D., and Stephanopoulos, G. (1998) *Eur. J. Biochem.* **252**, 360–371
- Schmidt, K., Carlsen, M., Nielsen, J., and Villadsen, J. (1997) *Biotechnol. Bioeng.* **55**, 831–840
- Murphy, D. J., and Cummis, I. (1989) *J. Plant Physiol.* **135**, 63–69
- Norton, G. (1989) in *Oil Crops of the World* (Röbbelen, G., Downey, R. K., and Ashri, A., eds) pp. 165–191, McGraw-Hill Inc., New York
- Murphy, D. J., Keen, J. N., Osullivan, J. N., Au, D. M. Y., Edwards, E. W., Jackson, P. J., Cummis, I., Gibbons, T., Shaw, C. H., and Ryan, A. J. (1991) *Biochim. Biophys. Acta* **1088**, 86–94
- Katz, J., and Wood, H. G. (1960) *J. Biol. Chem.* **235**, 2165–2177
- Katz, J., and Rognstad, R. (1967) *Biochemistry* **6**, 2227–2247
- Wiechert, W., Mollney, M., Petersen, S., and de Graf, A. A. (2001) *Metab. Eng.* **3**, 265–283
- Agrawal, P. K., and Calvin, D. T. (1971) *Can. J. Bot.* **49**, 267–272
- Scheibe, R. (1991) *Plant Physiol.* **96**, 1–3
- Heineke, D., Riens, B., Grosse, H., Hoferichter, P., Peter, U., Fluegge, U. I., and Heldt, H. W. (1991) *Plant Physiol.* **95**, 1131–1137
- Asokanathan, P. S., Johnson, R. W., Griffith, M., and Krol, M. (1997) *Physiol. Plant.* **101**, 353–360
- Thom, E., Mohlmann, T., Quick, W. P., Camara, B., and Neuhaus, H. E. (1998) *Planta* **204**, 226–233
- Anderson, L. E. (1981) *Biochem. Biophys. Res. Commun.* **99**, 1199–1202
- Hartwell, J., Bowsher, C. G., and Emes, M. J. (1996) *Planta* **200**, 107–112